



Cite as
Nano-Micro Lett.
(2019) 11:26

Received: 18 January 2019
Accepted: 21 February 2019
© The Author(s) 2019

Origin of Luminescent Centers and Edge States in Low-Dimensional Lead Halide Perovskites: Controversies, Challenges and Instructive Approaches

Jiming Bao^{1,2,3} ✉, Viktor G. Hadjiev^{4,5} ✉

✉ Jiming Bao, jbao@uh.edu; Viktor G. Hadjiev, vhadjiev@uh.edu

¹ Department of Electrical and Computer Engineering, University of Houston, Houston, TX 77204, USA

² Department of Chemistry, University of Houston, Houston, TX 77204, USA

³ Materials Science and Engineering, University of Houston, Houston, TX 77204, USA

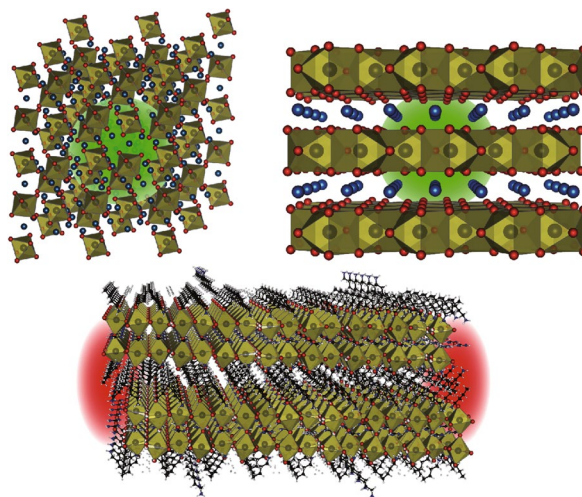
⁴ Texas Center for Superconductivity, University of Houston, Houston, TX 77204, USA

⁵ Department of Mechanical Engineering, University of Houston, Houston, TX 77204, USA

HIGHLIGHTS

- Controversial luminescent centers and edge states in low-dimensional perovskites were summarized.
- Evaluated experimental evidences and discussed the root cause for challenges and controversies.
- New experimental techniques were suggested to resolve the controversies and identify the nature of luminescent centers.

ABSTRACT With only a few deep-level defect states having a high formation energy and dominance of shallow carrier non-trapping defects, the defect-tolerant electronic and optical properties of lead halide perovskites have made them appealing materials for high-efficiency, low-cost, solar cells and light-emitting devices. As such, recent observations of apparently deep-level and highly luminescent states in low-dimensional perovskites have attracted enormous attention as well as intensive debates. The observed green emission in 2D CsPb₂Br₅ and 0D Cs₄PbBr₆ poses an enigma over whether it is originated from intrinsic point defects or simply from highly luminescent CsPbBr₃ nanocrystals embedded in the otherwise transparent wide band gap semiconductors. The nature of deep-level edge emission in 2D Ruddlesden–Popper perovskites is also not well understood. In this mini review, the experimental evidences that support the opposing interpretations are analyzed, and challenges and root causes for the controversy are discussed. Shortcomings in the current density functional theory approaches to modeling of properties and intrinsic point defects in lead halide perovskites are also noted. Selected experimental approaches are suggested to better correlate property with structure of a material and help resolve the controversies. Understanding and identification of the origin of luminescent centers will help design and engineer perovskites for wide device applications.



KEYWORDS Low-dimensional perovskites; Luminescent centers; Edge states; Cesium lead halides; Deep-level states; Ruddlesden–Popper perovskites



1 Introduction

Lead halide perovskites have provided us not only a long-awaited material platform to realize the dream of high-efficiency solar cells and many other optoelectronic devices, but also a wide range of structures to explore unusual fundamental sciences [1–5]. Depending on spatial configurations, lead halide octahedrons can form structures from three-dimensional (3D) all the way to 0D perovskites [6]. While still not completely understood, the superior optoelectronic properties of perovskites are believed to originate from their immunity to defects and lack of non-radiative deep-level traps, which have made them ideal materials for high-efficiency low-cost solar cells and many other optoelectronic devices [1–5, 7]. This is another reason why recent observations of possible new types of luminescent states in low-dimensional perovskites are surprising; in particular, they have been used for higher efficient solar cells and even brighter light-emitting diodes [6, 8–18]. Such apparent deep-level luminescent centers have been observed in 2D CsPb_2Br_5 [19–24] and 0D Cs_4PbBr_6 [11, 15, 16, 25, 26]. Because of their optical property similarities to those of CsPbBr_3 [27–29], the emission is believed to originate from embedded CsPbBr_3 nanocrystals [15, 16, 30–36]. But many other researchers attribute it to intrinsic point defects because no CsPbBr_3 nanocrystals have been found in their emissive samples [11, 25, 26]. The debates on the origin of Cs_4PbBr_6 are especially hot, as seen from four recent articles which acknowledge the controversy but are inclined to support one over the other [15, 16, 25, 26]. Similar deep-level luminescence centers have also been observed in low-dimensional organic–inorganic metal halide materials with better pronounced morphological dimensionality [37, 38] than that in Cs–Pb–Br system. The study of luminescence centers in structurally simpler all-inorganic lead halide perovskites, however, is expected to be instructive for further understanding the origin of these centers in all types of metal halide perovskites. As perovskites bring us more interesting properties and have found wide device applications, it is essential to understand the nature and mechanism for these luminescent centers.

In this mini review, the experimental evidences that support the opposing interpretations of the luminescence centers in Cs–Pb–Br system are analyzed, and challenges and root causes for the controversy are discussed. Selected

experimental approaches are suggested to better correlate property with structure of a material and help resolve the controversies.

2 Defects and Inclusions in Cs–Pb–Br System Rooted in the Ternary Phase Diagram

The perovskite-like compounds in Cs–Pb–Br system, CsPbBr_3 , CsPb_2Br_5 and Cs_4PbBr_6 , can be easily synthesized via solution process or melt-grown [11, 19, 34, 39–42]. The possibility of the different phase coexistence is well expected, and the compounds are stable within narrow chemical potential ranges as shown by recent density functional theory (DFT) simulations [26].

The ternary phase diagram of the Cs–Pb–Br system shown in Fig. 1b demonstrates that the three different perovskite-like structures can be produced using only CsBr and PbBr_2 precursors. The different phases in Cs–Pb–Br system are grown by varying the precursor ratio (CsBr: PbBr_2). As shown in Ref. [43], slight change of the crystal growth conditions and controlled precursor ratios can produce the low-dimensional phases CsPb_2Br_5 and Cs_4PbBr_6 .

The 3D perovskite CsPbBr_3 is the only compound in Cs–Pb–Br system that produces inherent green PL emission. This perovskite material was found unstable in moisture environment, and its instability has been used successfully to transform it into the lower dimension but stable phases CsPb_2Br_5 [20, 23] and Cs_4PbBr_6 [44] in water environment. The water-induced transformation of CsPbBr_3 into CsPb_2Br_5 occurs in a sequential dissolution–recrystallization process under PbBr_2 -rich conditions [20]. Thus, synthesized CsPb_2Br_5 emits green photoluminescence (PL) with high PL quantum yield [20], but another approach using water was capable of growing non-emissive single crystals [23]. These observations hint that the green PL in CsPb_2Br_5 is likely due to highly luminescent CsPbBr_3 nanocrystal remnants.

Zhang et al. [44] have grown successfully a millimeter-sized Cs_4PbBr_6 bulk single crystal in concentrated CsBr aqueous solution that lacks green luminescence emission [44]. In the same work, they also demonstrate that vacuum annealing treatment activates green PL in original nongreen-luminescent Cs_4PbBr_6 crystals, which was attributed to the possible formation of CsPbBr_3 . A reversible phase transformation between CsPbBr_3 and CsPb_2Br_5

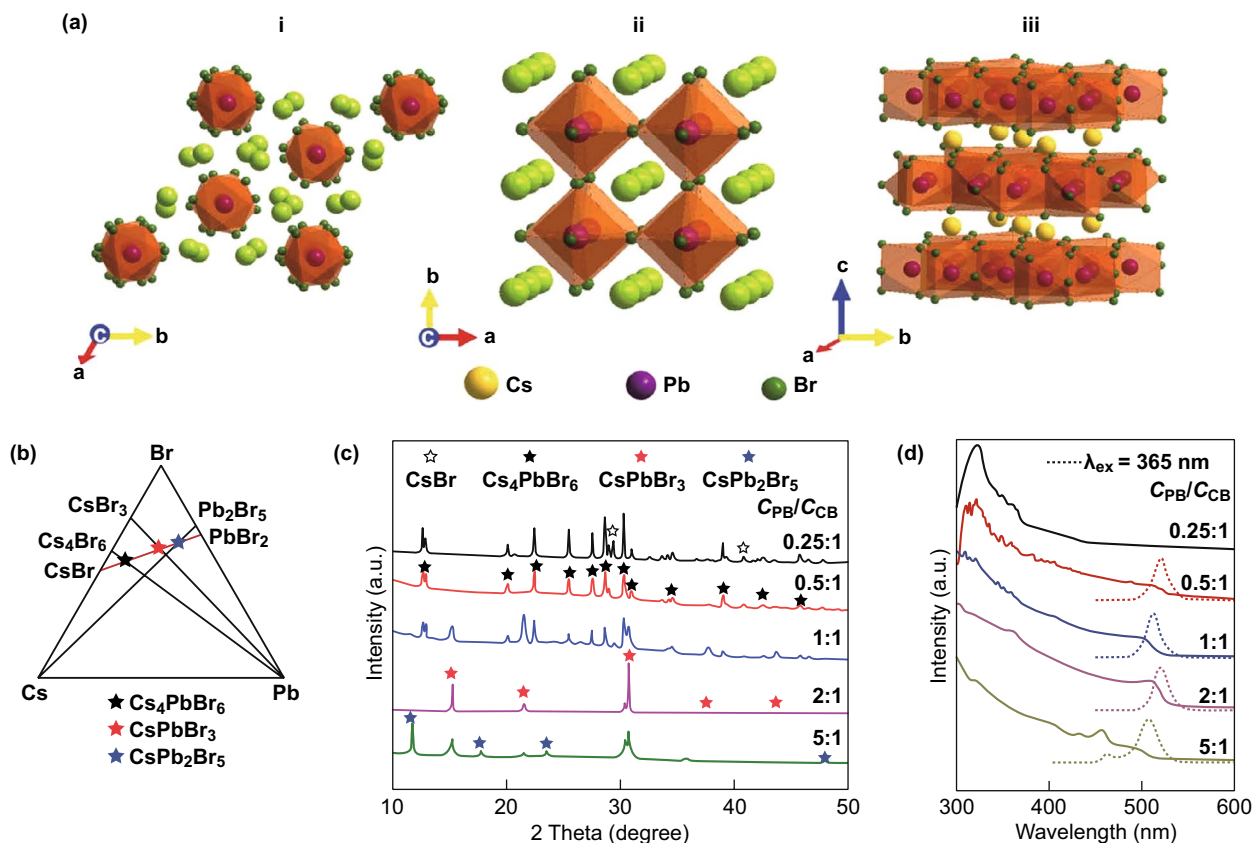


Fig. 1 Influence of $C_{PB}:C_{CB}$ ($C_{PB} = \text{PbBr}_2$, $C_{CB} = \text{CsBr} = 0.04 \text{ M}$) on the composition and optical properties of Cs–Pb–Br nanocrystals. **a** Crystal structure of Cs_4PbBr_6 (i), CsPbBr_3 (ii) and CsPb_2Br_5 (iii). **b** Ternary phase diagram of Cs, Pb and Br elements. Cs_4PbBr_6 , CsPbBr_3 and CsPb_2Br_5 fall on the line connecting PbBr_2 and CsBr in the diagram. **c** XRD results at different $C_{PB}:C_{CB}$. **d** PL and UV–Vis absorption spectra of the nanocrystals prepared at different $C_{PB}:C_{CB}$. The excitation wavelength for PL spectra is 365 nm. Reprinted with permission from Ref. [43]. Copyright 2018 Royal Society of Chemistry

nanosheets under intense laser light has been demonstrated in Ref. [45]. Therefore, the narrow phase stability regions in the ternary phase diagram and the possibility of partially reversible phase transformations strongly support the expectations for foreign phase inclusions in the Cs–Pb–Br compounds.

2.1 Luminescent State in 2D Wide Bandgap CsPb_2Br_5

CsPb_2Br_5 is a layered lead halide structure with Pb–Br framework separated by Cs layers (Fig. 2a). 2D CsPb_2Br_5 has also attracted a lot of attention recently due to many conflicting reports on its luminescence although it was synthesized and studied long ago [41, 46]. Zhang et al. [21] were the first to report the beneficial effect of CsPb_2Br_5 to 3D all-inorganic perovskite CsPbBr_3 : the attachment of

CsPb_2Br_5 nanoparticles to CsPbBr_3 nanocrystals enhanced PL of CsPbBr_3 by several folds and external quantum efficiency of CsPbBr_3 light-emitting diodes (LEDs) by 50%. Figure 2b, c shows that more than 90% of CsPbBr_3 are covered by CsPb_2Br_5 nanoparticles, but the PL and PLQY of $\text{CsPb}_2\text{Br}_5/\text{CsPbBr}_3$ are nearly the same as those of pure CsPbBr_3 nanocrystals. Figure 2d, e shows that these nanoparticles are not single phase, and high-resolution TEM reveals that they are $\text{CsPb}_2\text{Br}_5/\text{CsPbBr}_3$ nanocomposites with dark smaller CsPb_2Br_5 nanocrystals attached to larger CsPbBr_3 nanoparticles [21].

Shortly after that, Wang and co-workers reported nearly 90% quantum efficiency of pure CsPb_2Br_5 nanoplatelets and subsequently expanded their emission wavelength to whole visible spectrum using ion exchange with I and Cl [19] (Fig. 3). Note that the purity of the initial CsPb_2Br_5 and ion-exchanged nanocrystals was verified by XRD and

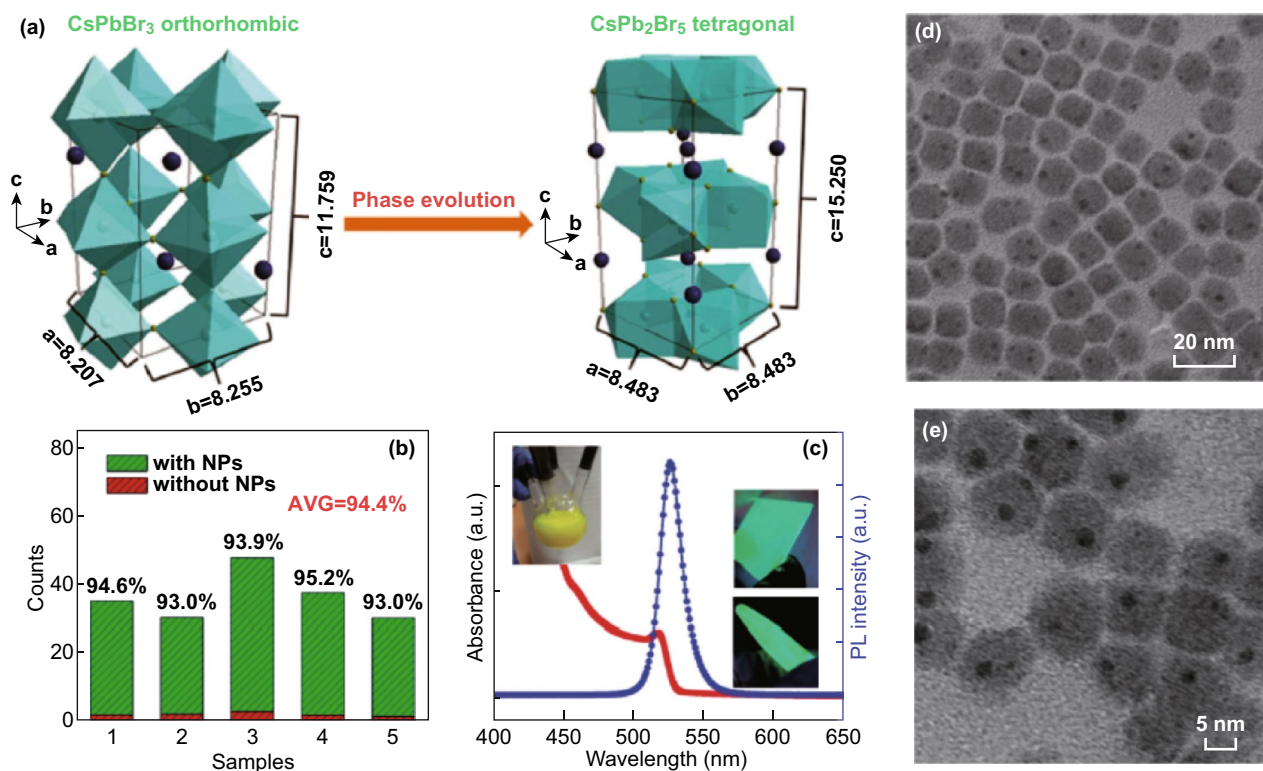


Fig. 2 **a** Crystal structure schematics of the orthorhombic CsPbBr₃ and tetragonal CsPb₂Br₅ (blue ball: Cs⁺). The unit of all the cell parameters is Å. Reprinted with permission from Ref. [22]. Copyright 2016 Royal Society of Chemistry. **b** The percentage of the CsPbBr₃ nanocrystal being covered by CsPb₂Br₅ nanoparticles and their PL quantum yield (PLQY). **c** Absorption and PL spectra of CsPb₂Br₅/CsPbBr₃ composites. The inset shows as-obtained products in four-necked flask and light emission of CsPb₂Br₅/CsPbBr₃ deposited on the glass and tube excited with ultraviolet light. **d–e** TEM images of all-inorganic CsPb₂Br₅/CsPbBr₃ nanocomposite at different magnifications. Dark dots in **e** are CsPb₂Br₅ nanoparticles. Reprinted with permission from Ref. [21]. Copyright 2016 Wiley–VCH

high-resolution TEM. Since then, many groups reported strong visible photoluminescence, high-efficiency LEDs, photodetectors and even lasing action in CsPb₂Br₅ microplates [20, 47–54]. Highly luminescent CsPb₂Br₅ nanowires with mixed halides are also synthesized recently [55].

Despite numerous reports, the claim of highly luminescent CsPb₂Br₅ has been met with skeptics. Li et al. [22] synthesized CsPb₂Br₅ nanosheets from CsPbBr₃ nanocubes. They have found that as the reaction goes on, both absorption and PL near 520 nm disappear, and the final product of CsPb₂Br₅ nanosheets displays no PL at all (Fig. 4). They also performed DFT simulation. The results (Fig. 4c, d) agree with the observation that CsPb₂Br₅ is an indirect wide band gap semiconductor [22].

The non-emissive nature of CsPb₂Br₅ can be best verified from transparent large-sized sheets in Fig. 5a, b [12, 13]. Emissive macro- or micro-CsPb₂Br₅ typically exhibits a characteristic yellow color as shown in Fig. 3a. Different

colors of CsPb₂Br₅ sheets in Fig. 5b are due to their thickness-dependent optical interference under ambient or white light. As CsPb₂Br₅ can be produced by converting CsPbBr₃ particles, CsPbBr₃ particles can be recovered from CsPb₂Br₅ as well. Figure 5c shows the evolution of XRD patterns when high-purity CsPb₂Br₅ (black) was annealed at 220 °C (red) and 400 °C (blue). As the annealing temperature increases, X-ray pattern of CsPbBr₃ particles begins to appear. This observation is also confirmed by TEM. Figure 5d, e shows CsPbBr₃ particles attached on CsPb₂Br₅ in sample annealed at 400 °C. The change can also be seen in the PL spectra. The redshift of the PL band with annealing temperature is due to increasing size of CsPbBr₃ particles [14]. Clearly, embedded CsPbBr₃ particles in CsPb₂Br₅ can be a source for green PL emission in otherwise non-emissive pure CsPb₂Br₅. However, the same group has changed their mind and considered green emission as an intrinsic property of CsPb₂Br₅ after synthesizing

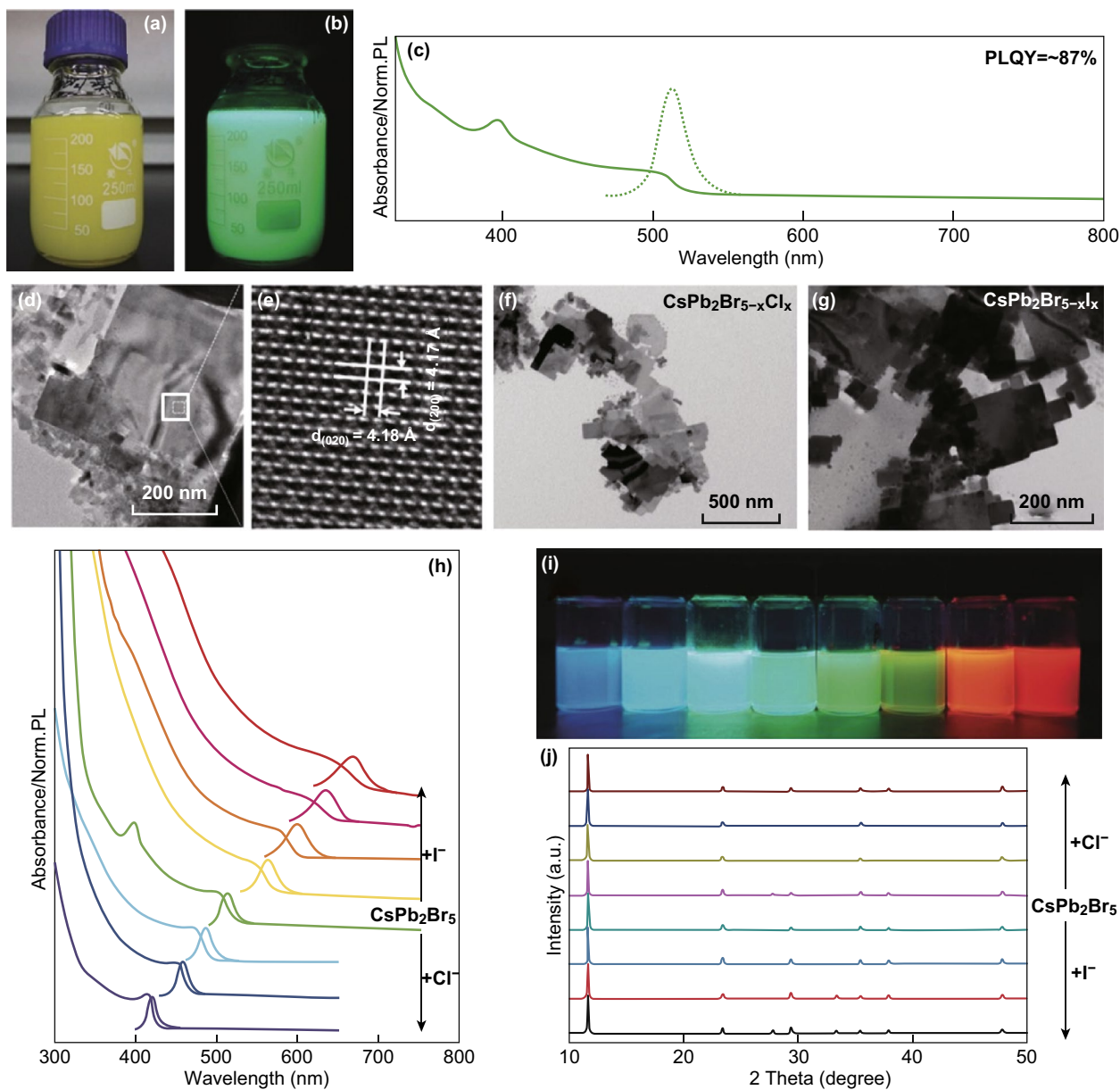


Fig. 3 **a, b** Photographs of as-obtained colloidal CsPb_2Br_5 nanoplatforms suspension under ambient conditions and the UV light (365 nm) irradiation, respectively. **c** Absorption and PL spectrum of CsPb_2Br_5 nanoplatforms in toluene solution. **d, e** TEM and HRTEM images of CsPb_2Br_5 nanoplatforms, respectively. **f, g** TEM images of representative nanostructures of $\text{CsPb}_2\text{Br}_{5-x}\text{Cl}_x$ and $\text{CsPb}_2\text{Br}_{5-x}\text{I}_x$, respectively. **h** Evolution of the optical absorption and PL spectra of CsPb_2Br_5 nanoplatforms with increasing quantities of anion exchange of I^- and Cl^- , respectively. **i, j** Corresponding photographs and powder XRD of the parent CsPb_2Br_5 nanoplatform and anion-exchanged samples. Reprinted with permission from Ref. [19]. Copyright 2016 Wiley-VCH

and analyzing green emissive CsPb_2Br_5 . Due to this reason, the mechanism for the green emission in CsPb_2Br_5 remains controversial. Many groups are aware of this controversy but are not able to support either of these two opposing claims [56–58].

2.2 Luminescent State in 0D Wide Bandgap Cs_4PbBr_6 Perovskite

In Cs_4PbBr_6 , PbBr_6 octahedrons are isolated by surrounding Cs ions and each octahedron behaves as a single molecular quantum dot (Fig. 6a inset), so Cs_4PbBr_6 is called 0D

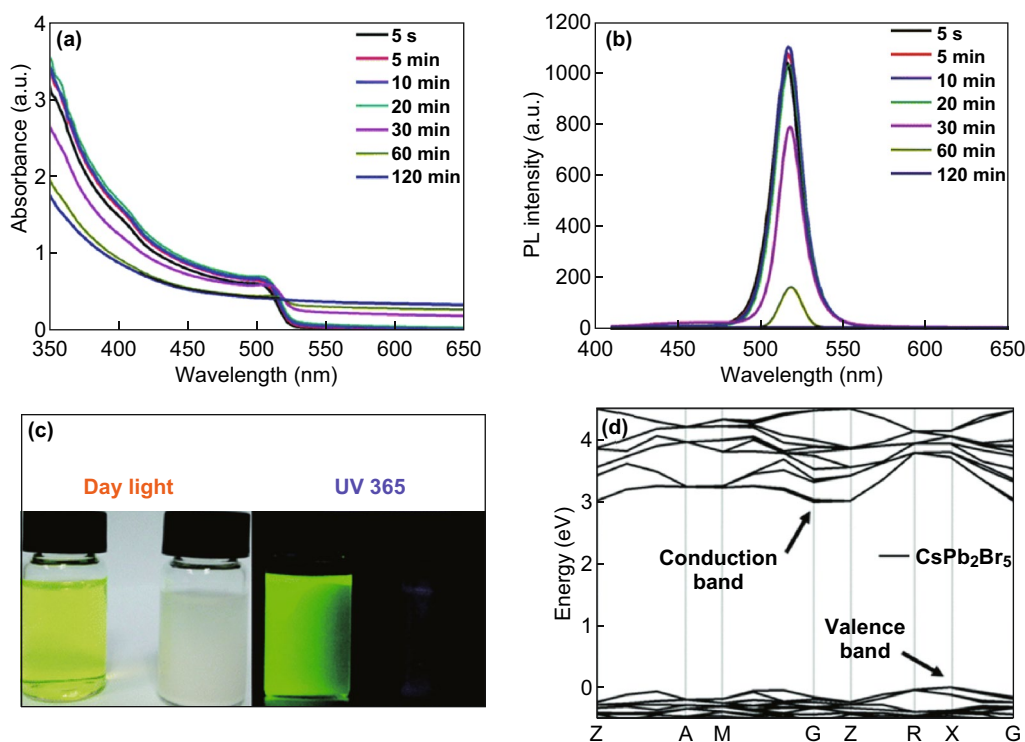


Fig. 4 Synthesis of non-emissive CsPb_2Br_5 nanosheets from CsPbBr_3 nanocubes. **a, b** Disappearance of absorbance and PL as the reaction time increases. **c** CsPbBr_3 nanocube solution (after 5 s reaction time) and CsPb_2Br_5 nanosheet suspension (after 2 h reaction time) in toluene under daylight (left) and a UV lamp (365 nm, right). **d** Calculated electronic band structure of CsPb_2Br_5 . Reprinted with permission from Ref. [22]. Copyright Royal Society of Chemistry

perovskite [15]. On the other hand, the crystallization of Cs_4PbBr_6 in a structure with translational symmetry and fixed orientation of PbBr_6 octahedrons to each other clearly indicate that the spacing between PbBr_6 is not enough to completely deactivate the interaction between them [16]. These interactions are better suppressed in the organic 0D metal halide hybrids [59, 60], which are closer to a quantum dot material. DFT calculations of an isolated Cs_4PbBr_6 structure, however, yield an energy gap close to those of bulk Cs_4PbBr_6 [61], which justifies the assignment of Cs_4PbBr_6 to 0D materials. Specifically, Cs_4PbBr_6 has attracted a lot of attention because of the high PL quantum efficiency reported in Ref. [11]. Figure 6 shows that Cs_4PbBr_6 also emits green light with a wavelength very close to that of CsPbBr_3 , but the PLQY is more than two orders of magnitude larger. Because Cs_4PbBr_6 is purified by dissolving CsPbBr_3 contamination using dimethyl sulfoxide (DMSO), and no X-ray of CsPbBr_3 is detected, the green emission is considered as an intrinsic property of Cs_4PbBr_6 [11]. Such strong green emission was initially attributed to the high exciton binding energy in

isolated PbBr_6 [11]. Later, an alternative explanation suggests that the green emission is due to a phonon-assisted transfer of photoexcited electrons to a charge-transfer state of Pb ions in the host lattice distorted by atomic displacements involved in the phonon [62]. Recently, the group published a series of papers and attributed the PL to intrinsic Br vacancies [26, 62–65]. Their theory has been supported by DFT calculations [26, 63] and other groups [25, 66–69].

The claim that the green PL emission is an intrinsic property of Cs_4PbBr_6 is also supported by the synthesis of large-sized single crystals (Fig. 7a, b). However, many other researchers do not agree with their observations and explanation [30–32, 44, 71]. Because the emission wavelength overlaps with that of CsPbBr_3 very well, it has been believed that the strong PL originates from embedded CsPbBr_3 nanocrystals. This alternative idea of non-intrinsic luminescent property is supported by the synthesis of non-emissive Cs_4PbBr_6 , both large-sized single crystals (Fig. 7c) and nanocrystals [30, 44, 62, 71]. Opposing simulations also show that the Br vacancies cannot produce such deep-level defect states [5,

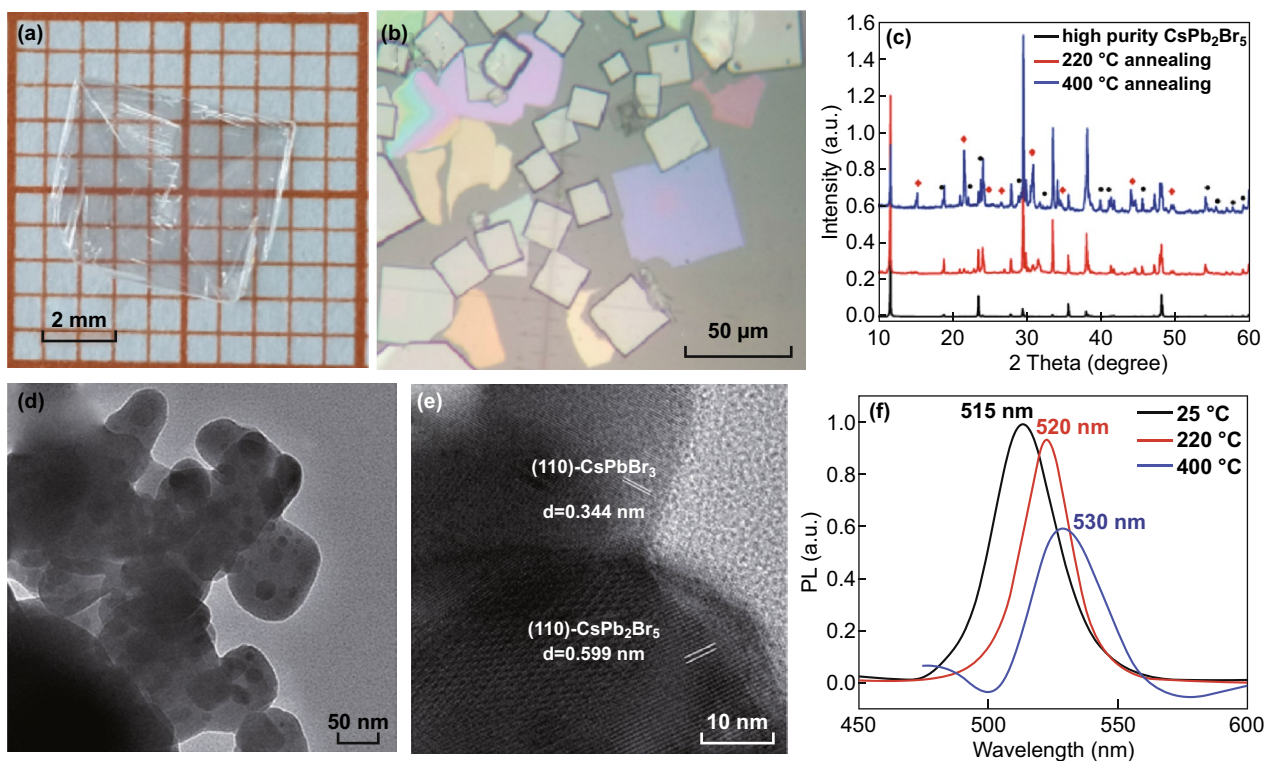


Fig. 5 **a** A transparent colorless CsPb_2Br_5 crystal with an area of up to $5 \times 5 \text{ mm}^2$. **b** CsPb_2Br_5 flakes on sapphire. The thickness of the purple crystal is only 160 nm [13]. **c** Powder XRD pattern of CsPb_2Br_5 particles after annealing at different temperatures (red squares represent CsPbBr_3 (PDF#18-0364), black dots represent PbBr_2). **d** Low-resolution and **e** high-resolution TEM image of a representative CsPb_2Br_5 cluster after annealing at 400 °C. **f** PL spectra of the three CsPb_2Br_5 samples characterized by XRD in **c** under 400 nm excitation [14]. Reprinted with permission from Refs. [13, 14]. Copyright 2017–2018 Royal Society of Chemistry

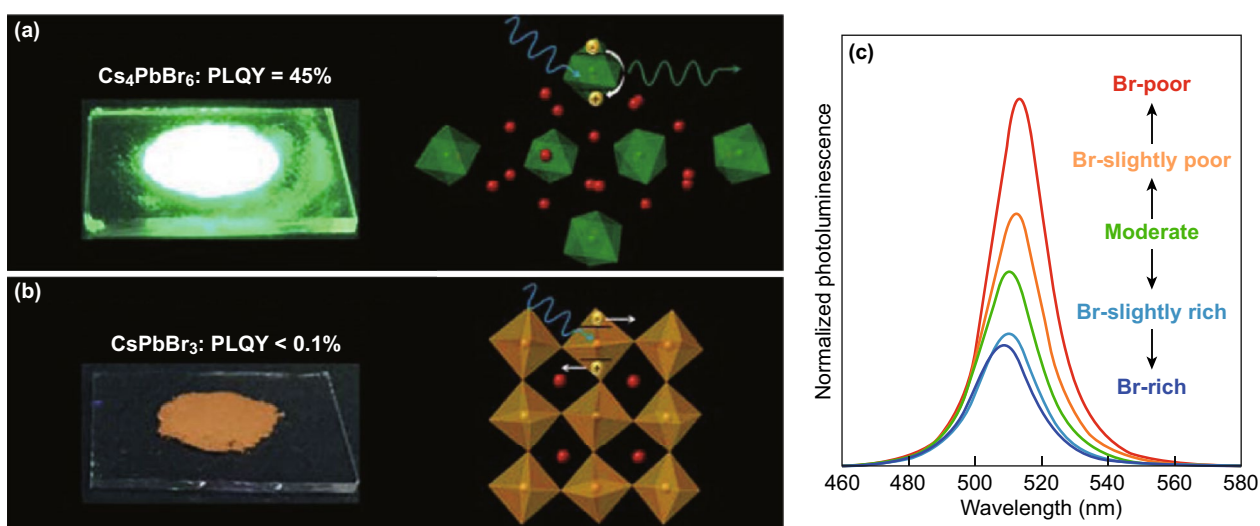


Fig. 6 **a, b** CsPbBr_3 and Cs_4PbBr_6 powders on the glass slides under UV light (365 nm). Insets are schematics of their crystal structures [11]. **c** PL intensity as a function of excitation wavelengths for Cs_4PbBr_6 , (normalized PL spectra according to the absorbance at an excitation wavelength of 375 nm) [26]. Reprinted with permission from Refs. [11, 26]. Copyright American Chemical Society

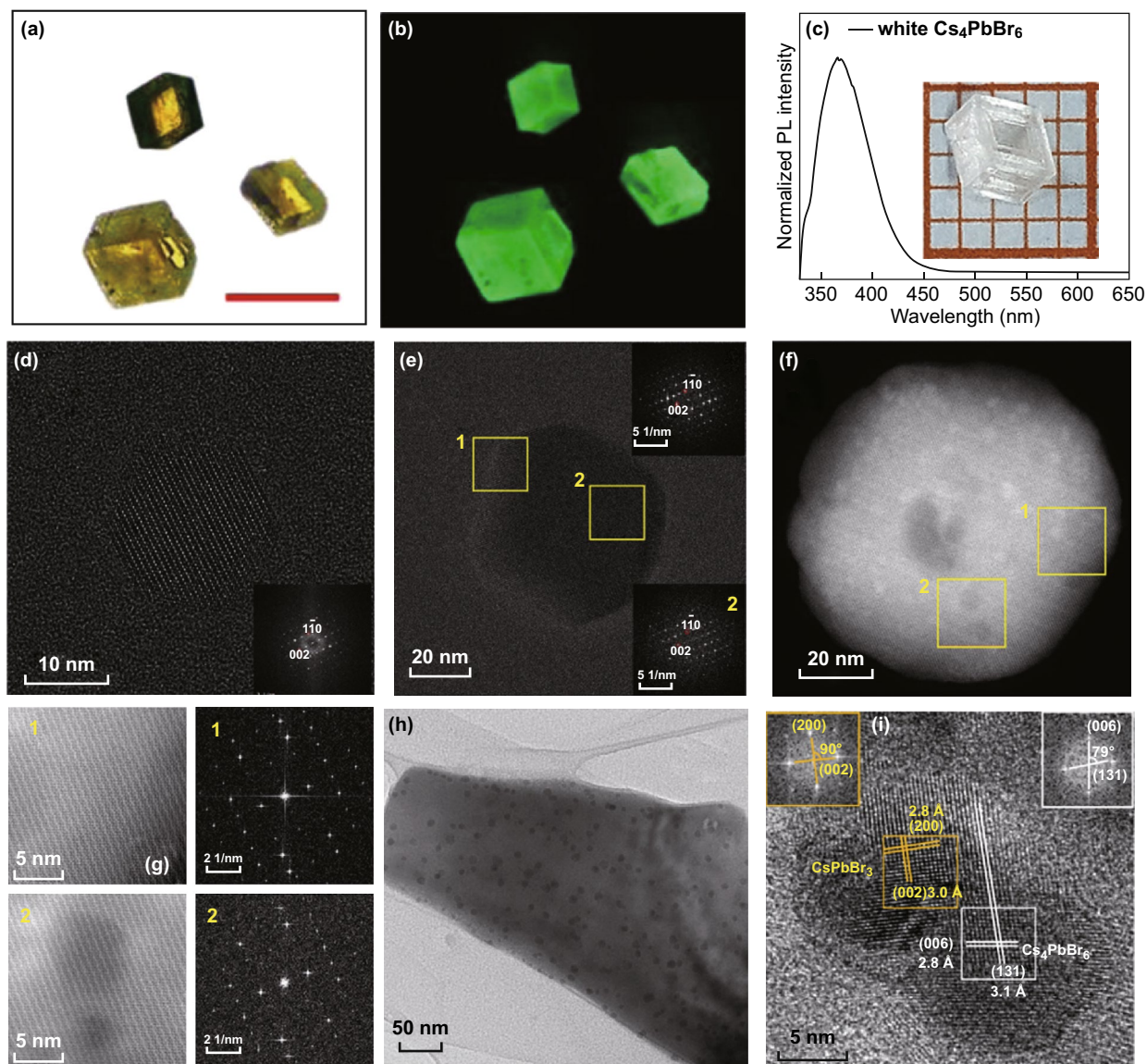


Fig. 7 **a, b** Optical and fluorescent microscope pictures of emissive Cs₄PbBr₆ single crystals. Scale bar: 500 μm [63]. **c** Photograph of a millimeter-sized non-emissive Cs₄PbBr₆ single crystal. Inset: PL spectrum [44]. **d–g** Drift-corrected HRTEM images of **d** a non-emissive and **e** a green emissive Cs₄PbBr₆ nanocrystals. The FFT patterns are shown as insets. **f** High-angle annular dark field (HAADF)-STEM image of a green emissive Cs₄PbBr₆ nanocrystal and **g** HAADF-STEM images and FFT patterns of selected areas 1 and 2 in **f** [26]. **h** TEM and **i** HRTEM images of CsPbBr₃ nanocrystals in the Cs₄PbBr₆ matrix. The insets show the FFT images [70]. Reprinted with permission from Refs. [26, 44, 63, 70]. Copyright American Chemical Society

[15, 16, 33]. As the strongest experimental evidences, both sides show high-resolution TEM images. Figure 7d–g compares TEM images of emissive and non-emissive Cs₄PbBr₆ nanocrystals. Both types of nanocrystals exhibit clean single crystal structure, and no CsPbBr₃ inclusion is found. On the other hand, CsPbBr₃/Cs₄PbBr₆ nanocomposites have been frequently synthesized and observed, and they exhibit strong PLQY as expected [16, 34, 70, 72].

2.3 Bright Edge States in 2D Ruddlesden–Popper (R–P) Perovskites

Corner-sharing PbBr₆ octahedrons as those in CsPbBr₃ are definitely the structures that can produce visible PL. This has also been confirmed by the PL properties of two-dimensional (2D) R–P lead halide perovskites [10]. The observed

crystal edge bright PL emission, different from that of the bulk one, in these materials is very instructive with demonstrated effects of PbBr_6 framework relaxation at the surface of perovskite crystals.

A surface is an inevitable termination of periodic lattices of any single crystals even when we are only interested in their bulk properties. For 2D materials, edges will become surfaces and introduce surface defects as they terminate their 2D expansion. A surface will typically introduce detrimental or unwanted effects to the bulk materials so that surface treatment or passivation is crucial for the desired function or performance of materials. Because of this reason, it was

very surprising that the edges of 2D organic–inorganic perovskites provide a deep-level luminescent center that also enhances the performance of solar cells [10].

In 2017, Blancon et al. [10] reported that 2D R–P perovskites $(\text{BA})_2(\text{MA})_{n-1}\text{Pb}_n\text{I}_{3n+1}$ exhibit a low energy photoluminescence in the edge of exfoliated flakes when n is 3 or larger (Fig. 8a–c). Their emission energy is ~ 300 meV below the band gap of $(\text{BA})_2(\text{MA})_{n-1}\text{Pb}_n\text{I}_{3n+1}$. Unlike conventional deep-level defect states, they can quickly dissociate photoexcited excitons and prevent electron–hole from non-radiative recombination [10]. By fabricating 2D platelets vertically and having edges directly connected to the electrodes, the

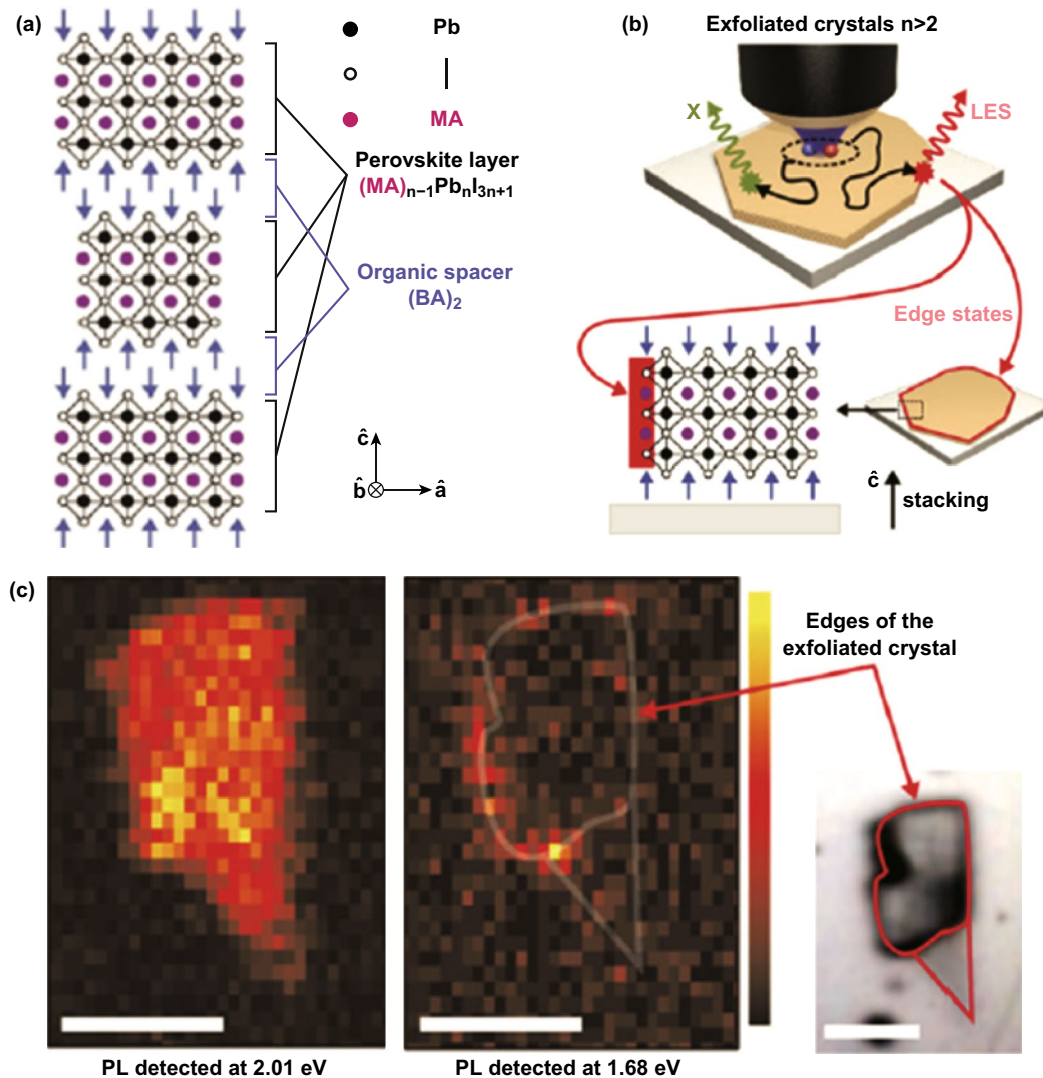


Fig. 8 Edge emission in $(\text{BA})_2(\text{MA})_{n-1}\text{Pb}_n\text{I}_{3n+1}$ 2D R–P perovskite with $n=3$. **a** Schematics of crystal structure. **b** Schematics of the photoabsorption and PL processes in 2D perovskite exfoliated crystals with $n > 2$. **c** Photoluminescence intensity map of a single exfoliated crystal. Scale bar is 10 μm . Reprinted with permission from Ref. [10]. Copyright American Association for the Advancement of Science

researchers have demonstrated 12% efficiency of 2D perovskite cells [10]. However, the nature of the edge states was not totally understood, and even their chemical composition and microscopic structure have not been experimentally identified in their initial report [10].

It was not until a year later that a theory paper was published and offered a model to explain the edge states [73]. The calculation shows that when $n > 2$, the strain caused by the interface between inorganic and organic spacers will be relaxed to the edge lattices, causing a large

lattice distortion (Fig. 9a). The distortion is large enough to create new localized state with energy much lower than the band gap [73]. However, there is still no experimental confirmation of the lattice distortion on the edge. A related paper was just published and reports the effect of organic spacer on the distortion of inorganic lattice in the surface of monolayer R-P perovskites [74]. Figure 9b–e demonstrates the sensitivity of electronic band structure to the Pb-I lattices and surface lattice relaxation. The edge emission was just confirmed in a very latest work [75].

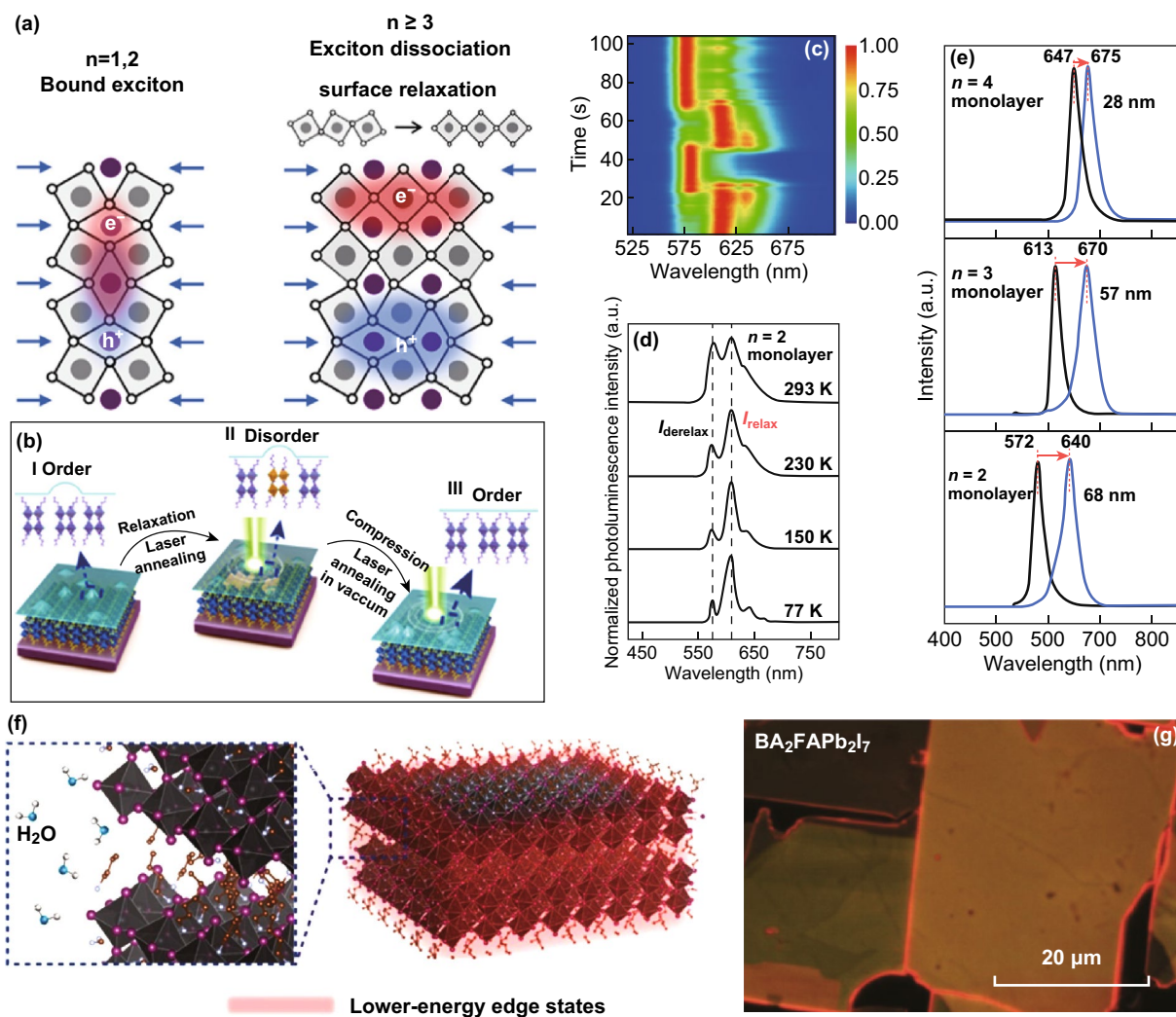


Fig. 9 **a** Schematics of the surface-induced exciton dissociation in R-P perovskites with $n \geq 3$. Reprinted with permission from Ref. [73]. Copyright American Chemical Society. **b** Schematic diagram showing the order–disorder transition by laser illumination. **c** Photoluminescence color map showing two continuous cycles of photoluminescence shifts during order–disorder transition, plotted as a function of laser irradiation time, emission wavelength and intensity. **d** Temperature-dependent changes in photoluminescence intensity. **e** Photoluminescence of $n=2$ –4 R-P perovskite monolayers. Black lines indicate the initial state photoluminescence, and blue lines are photoluminescence after relaxation. Reprinted with permission from Ref. [74]. Copyright Springer Nature. **f** Schematic of edge states of 2D halide perovskite due to moisture. **g** PL image of $\text{BA}_2\text{FAPb}_2\text{I}_7$ excited by UV light. Reprinted with permission from Ref. [75]. Copyright American Chemical Society

But as shown in Fig. 9f–g [75], the edge emission is not due to the intrinsic strain; rather, it is induced by water molecules. Furthermore, the edge emission can also be observed when $n = 2$. Again, these are just experimental observations, and the underlying structure and mechanism are still not clear and require further research.

3 Problems and Challenges in Revealing the Origin of Luminescence Centers in Lead Halide Perovskites

The current problems in identifying the origin of PL from in-gap luminescence centers are due to relatively large inconsistency in the results of both computational simulations and experimental characterization of lead halide perovskites. The basic properties of lead halide perovskites and expected intrinsic point defects have been studied extensively by using DFT. The first attempts of calculating the band structure of lead halide perovskites using local density functionals (LDA) and generalized gradient approximation (GGA) as GGA-PBE produced band gap values in accordance with the experimental ones. The top of valence band in Cs–Pb–Br 0D, 2D and 3D materials is composed of p -orbitals of Br with contribution from s -orbitals of Pb, whereas the bottom of conduction band is completely based on p -orbitals of Pb. Lead is a heavy metal known to possess strong spin–orbital coupling (SOC). The must-have inclusion of SOC in GGA-PBE calculations, however, results in a strong underestimate of band gap values in these materials. This also influences significantly the energy calculations of the native point defects (vacancies, interstitials and antisites) and defect complexes. The energy-level positions of different defects with respect to the band gap edges change with activating SOC. This makes quite dubious the assignment of certain defects as deep in-gap luminescence centers. The analysis of this problem has found its first solution in 2015 when Du [76] showed that the local density functionals used without SOC produce correct band gap values due to error cancelations [77], whereas inclusion of SOC involves self-interacting errors and requires the use of screened hybrid functionals as Heyd–Scuseria–Ernzerhof (HSE) to reproduce correctly both the band gap and the energy position of defects. Kang and Wang [5] presented the first complete calculations of the formation energy of all type point defects in CsPbBr₃ using

HSE + SOC. The formation energy of defects was calculated taking into account the Fermi energy and atomic chemical potentials of constituents [78, 79]. Although this work seems to deliver solid results, a few details are alarming and indicate that it may not be the final word on solving problems of modeling defects in lead halide perovskites.

The HSE functional includes a portion of non-local Hartree–Fock (HF) exchange in addition to local GGA-PBE one. The HSE functional partitions the Coulomb operator for a pair of charges into two ranges: short (SR) = $[1 - \text{erf}(\omega r)]/r$ and long (LR) = $\text{erf}(\omega r)/r$ that are defined and controlled by the range-separation parameter ω set empirically to 0.15 Bohr⁻¹ in the so-called HSE03 [80] version and to 0.11 Bohr⁻¹ in the HSE06 version. HSE incorporates 25% SR HF exchange (mixing parameter, $a = 0.25$), no LR HF exchange, 75% SR and full LR PBE exchange, and 100% PBE correlation. Test calculations using HSE03 [80] with $a = 0.25$ and $\omega = 0.15$ Bohr⁻¹ have reproduced well the band gap of a large number of semiconductors [81], that is, HSE is believed to be a universal functional. The band gap of CsPbBr₃, however, is calculated correctly using HSE + SOC only with HF exchange portion a set to 0.43 [5]. Recent extension of HSE + SOC to calculations of 2D CsPb₂Br₃ and 3D Cs₄PbBr₆ shows that there are no universal HSE06 parameters a and ω that produce the band gaps correctly for all Cs–Pb–Br compounds [26]. The band gap of CsPb₂Br₅ and Cs₄PbBr₆ is calculated to be close to the experimental one for $a = 0.2$ [26], that is, different from both $a = 0.43$ for CsPbBr₃ and most importantly different from $a = 0.25$ of the original HSE06 that has been claimed to be a universal for correct calculations of band gaps in semiconductors. One yet unexplored path is to repeat these calculations with fixed original $a = 0.25$ in HSE functional and varying the screen parameter ω and then find a physical reason for different screening parameters in Cs–Pb–Br compounds.

The DFT results of defect formation energy calculations of CsPbBr₃, CsPb₂Br₅ and Cs₄PbBr₆ and the defect energy levels with respect to the energy band gap in these compounds are shown in Fig. 10 [26]. The defect formation energy was calculated in a similar way as in Ref. [5], but the results for some of the defects in CsPbBr₃ are different in the two papers. No critical analysis has been done so far on whether this is the most reliable and realistic approach for calculations of the defect formation energy. Apart

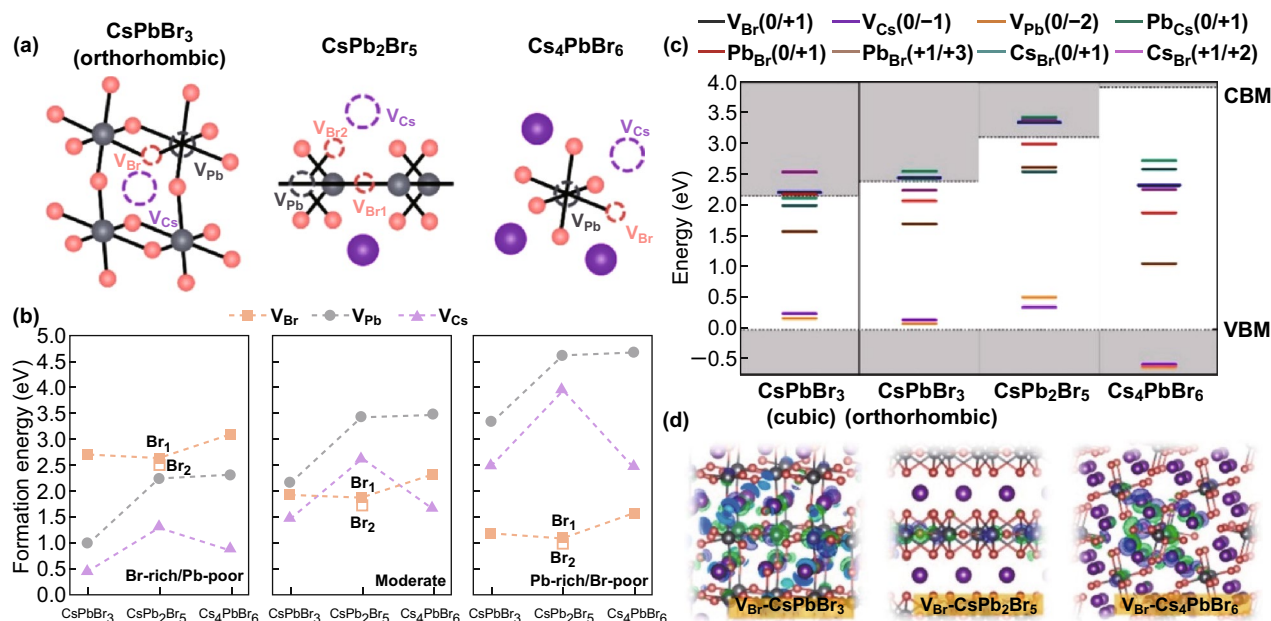


Fig. 10 **a** Illustrations of Br, Pb and Cs vacancies (V_{Br} , V_{Pb} and V_{Cs}). **b** Calculated defect formation energies for orthorhombic- $CsPbBr_3$, $CsPb_2Br_5$ and Cs_4PbBr_6 at Br-rich/Pb-poor, moderate and Pb-rich/Br-poor conditions. **c** Defect charge transition levels of $CsPbBr_3$, $CsPb_2Br_5$ and Cs_4PbBr_6 . **d** Charge density distributions of V_{Br} defect states for $CsPbBr_3$, $CsPb_2Br_5$ and Cs_4PbBr_6 calculated at the GGA/PBE level of theory. The band gaps were corrected using the HSE+SOC method. Reprinted with permission from Ref. [26]. Copyright American Chemical Society

from the supercell size-independent errors in these calculations as the choice of DFT functional and the choice of exchange correlation potentials discussed above, there are a number of supercell size-dependent errors, e.g., in Ref. [82], that have not been explored yet in the Cs–Pb–Br compounds. There is a need for a more rigorous approach to defect property calculations for the Cs–Pb–Br system in accordance with analyses and prescriptions given in Ref. [83].

The origin of green PL in Cs_4PbBr_6 is attributed to Br vacancies, V_{Br} (as in Ref. [26]). As shown in Fig. 10c, however, $V_{Br}(0/+1)$ cannot be involved in the green PL emission observed in $CsPb_2Br_5$. The only candidates for defect mediated PL in $CsPb_2Br_5$ are the antisites Pb_{Br} and Cs_{Br} . Another computational study of $CsPb_2Br_5$ [33], however, predicts the positions of unoccupied and occupied levels of $V_{Br}(0)$ to lay at ~ 0.25 and ~ 0.5 eV, respectively, below the conduction band edge. The puzzle of the very similar green PL in $CsPb_2Br_5$ and Cs_4PbBr_6 due to defects remains unsolved. These notes show the complexity involved in the

modeling of Cs–Pb–Br compounds and their native point defects and the degree of confidence one may have in the DFT results.

The arguments in favor of green PL in $CsPb_2Br_5$ and Cs_4PbBr_6 due to $CsPbBr_3$ nanocrystal inclusions are better justified experimentally than those in support of native point defects. Indeed, the studies of $CsPbBr_3$ absorption and emission spectra variation with nanocrystal size clearly show a quantum dot size effects with a PL peak position shift from 2.35 eV in bulk crystals to 2.7 eV in ~ 4 -nm crystal [28, 84].

The results in Fig. 11 show that typically observed green PL luminescence at 2.35–2.5 eV in $CsPb_2Br_5$ and Cs_4PbBr_6 may well be due to $CsPbBr_3$ nanocrystal inclusions in these wide band gap semiconductors. One way to move forward in revealing the nature of luminescence centers is to provide stronger experimental evidence on the nature of PL centers in Cs–Pb–Br system although this is also challenging as we discuss it below.

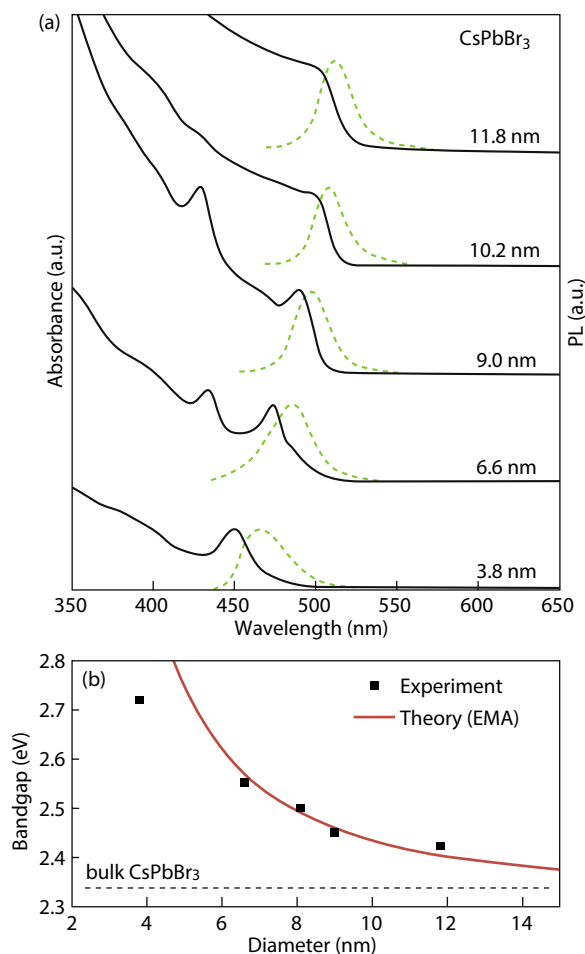


Fig. 11 **a** Quantum size effects in the absorption and emission spectra of 5–12-nm CsPbBr₃ NCs. **b** Experimental versus theoretical (effective mass approximation) size dependence of the band gap energy. Reprinted with permission from Ref. [28]. Copyright American Chemical Society

4 Designing Combined Experimental Characterization Approaches for Better Consistency

Structure–property relation is the major goal of materials science and engineering. Specifically for the Cs–Pb–Br system one of the important properties is the photoluminescence, while its structure is determined by XRD, TEM and Raman spectroscopy. The last one is an indirect structure-related technique. The major reasons for these structure–property controversies or challenges are the difference in probing length scale and sensitivity. XRD is an average technique and has relatively low phase detection sensitivity. It is sensitive to the minority phase domain

size, which below a few hundred nanometers usually diminishes and broadens the related XRD peaks, whereas PL can be emitted even from quantum dots and single molecular inclusions. TEM can provide detailed atomic structures, but there are two major difficulties. The first is that the size of PL and TEM probes are orders of magnitude different. TEM can only probe a much smaller sample, on the order of 100 nm in size; however, micro-PL still require a micrometer-sized sample. The second reason is that perovskite-like materials are very sensitive to electron beams and can get damaged easily, so the structure of perovskite is hard to be studied and advanced low-dose TEM is needed [65].

Raman is a well-established and sensitive technique to identify a material. In addition, Raman is compatible with PL and requires a small sample amount, so Raman can serve both the structure determination and property related to PL. For instance, the non-resonant Raman scattering is structure related, but at resonance it may probe electronic states that concurrently take part in PL. Raman and PL have been separately used in characterizing the luminescent centers, but they were only used for qualitative study, and a combined and calibrated Raman–PL has been missing. The key to such quantitative Raman–PL analysis is the calibrations of both Raman and PL using well-known reference materials. Note that PL is very sensitive to material quality, so a reference sample should be carefully chosen for the combined Raman and PL. For instance, CsPbBr₃ nanocrystals can have a PLQY of 60–90% [27–29], but the PLQY of CsPbBr₃ micropowders can be as low as 0.1%. CsPbBr₃ nanocrystals should be used to confirm whether they are the source for green emission. So far, a successful application of combined Raman/PL mapping of the same sample area of CsPb₂Br₅ was reported in Ref. [23]. In that study, the Raman spectroscopy distinguishes the single crystalline part of CsPb₂Br₅ [77], which turned out to be non-emissive, from the polycrystalline part that produces green PL.

The optical absorption spectra of Cs–Pb–Br compounds can indicate indirectly, but not for certain, whether the samples are PL emissive or not. A promising alternative approach reported in Ref. [31, 85] uses TEM for structural characterization and energy loss spectroscopy (EELS) in the low-loss region as equivalent of optical absorption in CsPbBr₃ and CsPbBr₃/Cs₄PbBr₆. The results of TEM–EELS characterization of CsPbBr₃/Cs₄PbBr₆ nanocrystals are

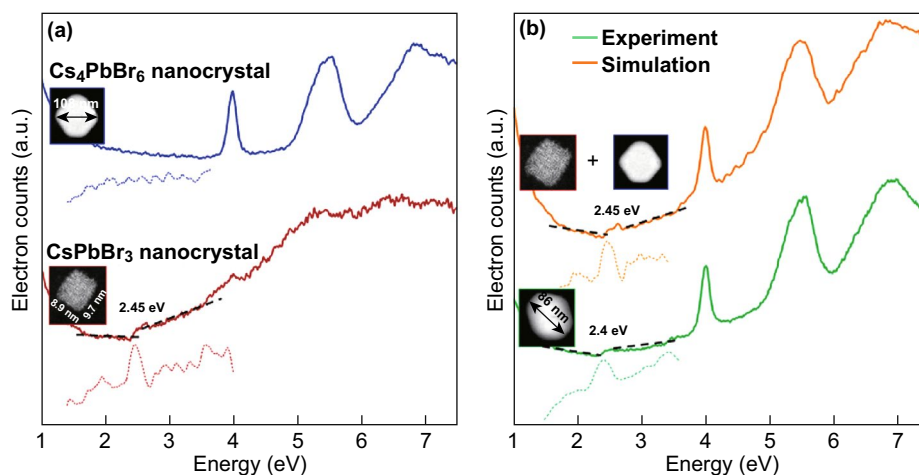


Fig. 12 Energy band gap and structure. **a** Valence-loss EEL spectra representing the absorption of a CsPbBr₃ nanocube (red spectrum) and a Cs₄PbBr₆ NC (blue), appearing in the same sample (160 °C). The band gap energy of the nanocube (2.45 eV) is determined from the peak of the first derivative of the EEL spectrum, which appears due to the abrupt onset in absorption (indicated by the dotted lines). No onset is observed for the Cs₄PbBr₆ NC which is an insulator with a large band gap energy of 4 eV. **b** Valence-loss EEL spectrum of a spherical nanocrystal (green) observed in the same sample, formed upon the hybridization of a nanocube and a nano-hexagon. The latter process is represented by the simulated EEL spectrum (orange) which is obtained from adding the experimentally obtained spectra of the nano-hexagon and nanocube as shown in **a**. The hybrid has, as expected, a band gap energy similar to that of the nanocube. Reprinted with permission from Ref. [31]. Copyright American Chemical Society

shown in Fig. 12. The main limitations of the EELS technique are the effect of sample thickness, relatively low sensitivity and energy resolution in the low-loss region when compared to optical spectroscopy.

The ultimate technique for structure–property relation is combined TEM-PL on a single nanocrystal [86]. The Raman scattering from ultra-small amount of highly luminescence compounds could be too weak to be detectable. A major challenge is to avoid electron beam-induced damages to perovskites. High-resolution TEM imaging has been used by competing sides to support their arguments, but no such combined study was reported. The observation of CsPbBr₃/Cs₄PbBr₆ nanocomposites certainly cannot exclude possible defect luminescent states; although no apparent CsPbBr₃ nanocrystal was found in some single crystals of emissive Cs₄PbBr₆, PL from the same nanocrystal was actually not demonstrated [19, 51, 55]. More importantly, PL should be performed before and after TEM imaging to ensure no damage has occurred. To reveal the origin of edge states in R–P perovskites [10, 75], the next step is to reproduce the reported results and further determine the factors that are responsible for the edge states. Besides the reported TEM and AFM [75], non-invasive techniques such as Raman and FTIR should be

used to identify the structural and chemical changes to the edge lattices [85, 87]. Note that nanometer scale versions of Raman and FTIR are already available to probe local structures [88, 89].

PL, Raman, XRD and TEM are passive techniques; new techniques that can apply external stimulus such as mechanical, electrical, or magnetic force to probe the dynamic response of luminescent centers and distinguish point defect from CsPbBr₃ nanocrystals are needed. The challenges and controversies in perovskites have also brought us a great opportunity to test new theory, develop new experimental techniques and eventually provide us new understanding and insight to develop and engineer better materials for a wide range of optoelectronic device applications.

Acknowledgements JM Bao acknowledges support from the Robert A. Welch Foundation (E-1728) and National Science Foundation (EEC-1530753). VG Hadjiev's work was supported by the State of Texas through the Texas Center for superconductivity at the University of Houston.

Open Access This article is distributed under the terms of the Creative Commons Attribution 4.0 International License (<http://creativecommons.org/licenses/by/4.0/>), which permits unrestricted use, distribution, and reproduction in any medium, provided you give appropriate credit to the original author(s) and the source,

provide a link to the Creative Commons license, and indicate if changes were made.

References

1. Y.X. Zhao, K. Zhu, Organic-inorganic hybrid lead halide perovskites for optoelectronic and electronic applications. *Chem. Soc. Rev.* **45**(3), 655–689 (2016). <https://doi.org/10.1039/c4cs00458b>
2. J. Huang, Y. Yuan, Y. Shao, Y. Yan, Understanding the physical properties of hybrid perovskites for photovoltaic applications. *Nat. Rev. Mater.* **2**, 17042 (2017). <https://doi.org/10.1038/natrevmats.2017.42>
3. J.W. Xiao, L. Liu, D.L. Zhang, N. De Marco, J.W. Lee, O. Lin, Q. Chen, Y. Yang, The emergence of the mixed perovskites and their applications as solar cells. *Adv. Energy Mater.* **7**, 1700491 (2017). <https://doi.org/10.1002/aenm.201700491>
4. H.M. Zhu, Y.P. Fu, F. Meng, X.X. Wu, Z.Z. Gong et al., Lead halide perovskite nanowire lasers with low lasing thresholds and high quality factors. *Nat. Mater.* **14**, 636–642 (2015). <https://doi.org/10.1038/nmat4271>
5. J. Kang, L.W. Wang, High defect tolerance in lead halide perovskite CsPbBr₃. *J. Phys. Chem. Lett.* **8**, 489–493 (2017). <https://doi.org/10.1021/acs.jpcclett.6b02800>
6. H.R. Lin, C.K. Zhou, Y. Tian, T. Siegrist, B.W. Ma, Low-dimensional organometal halide perovskites. *ACS Energy Lett.* **3**, 54–62 (2018). <https://doi.org/10.1021/acscenergyl.7600926>
7. D. Han, C.M. Dai, S.Y. Chen, Calculation studies on point defects in perovskite solar cells. *J. Semicond.* **38**, 011006 (2017). <https://doi.org/10.1088/1674-4926/38/1/011006>
8. S. Gonzalez-Carrero, R.E. Galian, J. Perez-Prieto, Organometal halide perovskites: bulk low-dimension materials and nanoparticles. *Part. Part. Syst. Charact.* **32**, 709–720 (2015). <https://doi.org/10.1002/ppsc.201400214>
9. K. Hong, Q.V. Le, S.Y. Kim, H.W. Jang, Low-dimensional halide perovskites: review and issues. *J. Mater. Chem. C* **6**, 2189–2209 (2018). <https://doi.org/10.1039/c7tc05658c>
10. J.C. Blancon, H. Tsai, W. Nie, C.C. Stoumpos, L. Pedesseau et al., Extremely efficient internal exciton dissociation through edge states in layered 2D perovskites. *Science* **355**, 1288–1291 (2017). <https://doi.org/10.1126/science.aal4211>
11. M.I. Saidaminov, J. Almutlaq, S. Sarmah, I. Dursun, A.A. Zhumekenov et al., Pure Cs₄PbBr₆: highly luminescent zero dimensional perovskite solids. *ACS Energy Lett.* **1**, 840–845 (2016). <https://doi.org/10.1021/acscenergyl.6b00396>
12. I. Dursun, M.D. Bastiani, B. Turedi, B. Alamer, A. Shkurenko et al., CsPb₂Br₅ single crystals: synthesis and characterization. *Chemsuschem* **10**, 3746–3749 (2017). <https://doi.org/10.1002/cssc.201701131>
13. Z. Zhang, Y. Zhu, W. Wang, W. Zheng, R. Lin, F. Huang, Growth, characterization and optoelectronic applications of pure-phase large-area CsPb₂Br₅ flake single crystals. *J. Mater. Chem. C* **6**, 446–451 (2018). <https://doi.org/10.1039/c7tc04834c>
14. J. Li, H.J. Zhang, S. Wang, D.B. Long, M.K. Li et al., Synthesis of all-inorganic CsPb₂Br₅ perovskite and determination of its luminescence mechanism. *RSC Adv.* **7**, 54002–54007 (2017). <https://doi.org/10.1039/c7ra10693a>
15. Q.A. Akkerman, A.L. Abdelhady, L. Manna, Zero-dimensional cesium lead halides: history, properties, and challenges. *J. Phys. Chem. Lett.* **9**, 2326–2337 (2018). <https://doi.org/10.1021/acs.jpcclett.8b00572>
16. D. Han, H.L. Shi, W.M. Ming, C.K. Zhou, B.W. Ma et al., Unraveling luminescence mechanisms in zero-dimensional halide perovskites. *J. Mater. Chem. C* **6**, 6398–6405 (2018). <https://doi.org/10.1039/c8tc01291a>
17. X.Z. Min, P.C. Zhu, S. Gu, J. Zhu, Research progress of low-dimensional perovskites: synthesis, properties and optoelectronic applications. *J. Semicond.* **38**, 011004 (2017). <https://doi.org/10.1088/1674-4926/38/1/011004>
18. R. Guo, Z.A. Zhu, A. Boulesbaa, F. Hao, A. Puzetky et al., Synthesis and photoluminescence properties of 2D phenethylammonium lead bromide perovskite nanocrystals. *Small Methods* **1**, 1700245 (2017). <https://doi.org/10.1002/smt.201700245>
19. K.H. Wang, L. Wu, L. Li, H.B. Yao, H.S. Qian, S.H. Yu, Large-scale synthesis of highly luminescent perovskite-related CsPb₂Br₅ nanoplatelets and their fast anion exchange. *Angew. Chem. Int. Ed.* **55**, 8328–8332 (2016). <https://doi.org/10.1002/anie.201602787>
20. B. Turedi, K.J. Lee, I. Dursun, B. Alamer, Z.N. Wu et al., Water-induced dimensionality reduction in metal-halide perovskites. *J. Phys. Chem. C* **122**, 14128–14134 (2018). <https://doi.org/10.1021/acs.jpcc.8b01343>
21. X.L. Zhang, B. Xu, J.B. Zhang, Y. Gao, Y.J. Zheng, K. Wang, X.W. Sun, All-inorganic perovskite nanocrystals for high-efficiency light emitting diodes: dual-phase CsPbBr₃–CsPb₂Br₅ composites. *Adv. Funct. Mater.* **26**, 4595–4600 (2016). <https://doi.org/10.1002/adfm.201600958>
22. G.P. Li, H. Wang, Z.F. Zhu, Y.J. Chang, T. Zhang, Z.H. Song, Y. Jiang, Shape and phase evolution from CsPbBr₃ perovskite nanocubes to tetragonal CsPb₂Br₅ nanosheets with an indirect bandgap. *Chem. Commun.* **52**, 11296–11299 (2016). <https://doi.org/10.1039/c6cc05877a>
23. Y. Wang, C. Wang, X. Su, V.G. Hadjiev, H.A.C. Benavides et al., Bright luminescent surface states on the edges of wide-bandgap two-dimensional lead halide perovskite. *arXiv: 1803.11490* (2018)
24. K.J.L.B. Turedi, I. Dursun, B. Alamer, Z. Wu, E. Alarousu et al., Water-induced dimensionality reduction in metal-halide perovskites. *J. Phys. Chem. C* **122**, 14128–14134 (2018). <https://doi.org/10.1021/acs.jpcc.8b01343>
25. S. Seth, A. Samanta, Photoluminescence of zero-dimensional perovskites and perovskite-related materials. *J. Phys. Chem. Lett.* **9**, 176–183 (2018). <https://doi.org/10.1021/acs.jpcclett.7b02931>
26. J. Yin, H. Yang, K. Song, A.M. El-Zohry, Y. Han, O.M. Bakr, J.L. Bredas, O.F. Mohammed, Point defects and green



- emission in zero-dimensional perovskites. *J. Phys. Chem. Lett.* **9**, 5490–5495 (2018). <https://doi.org/10.1021/acs.jpcclett.8b02477>
27. J.Z. Song, J.H. Li, X.M. Li, L.M. Xu, Y.H. Dong, H.B. Zeng, Quantum dot light-emitting diodes based on inorganic perovskite cesium lead halides (CsPbX_3). *Adv. Mater.* **27**, 7162 (2015). <https://doi.org/10.1002/adma.201502567>
 28. L. Protesescu, S. Yakunin, M.I. Bodnarchuk, F. Krieg, R. Caputo et al., Nanocrystals of cesium lead halide perovskites (CsPbX_3 , X = Cl, Br, and I): novel optoelectronic materials showing bright emission with wide color gamut. *Nano Lett.* **15**, 3692–3696 (2015). <https://doi.org/10.1021/nl5048779>
 29. H.C. Wang, S.Y. Lin, A.C. Tang, B.P. Singh, H.C. Tong et al., Mesoporous silica particles integrated with all-inorganic CsPbBr_3 perovskite quantum-dot nanocomposites (MP-PQDs) with high stability and wide color gamut used for backlight display. *Angew. Chem. Int. Ed.* **55**, 7924–7929 (2016). <https://doi.org/10.1002/anie.201603698>
 30. Z.K. Liu, Y. Bekenstein, X.C. Ye, S.C. Nguyen, J. Swabeck et al., Ligand mediated transformation of cesium lead bromide perovskite nanocrystals to lead depleted Cs_4PbBr_6 nanocrystals. *J. Am. Chem. Soc.* **139**, 5309–5312 (2017). <https://doi.org/10.1021/jacs.7b01409>
 31. C. de Weerd, J.H. Lin, L. Gomez, Y. Fujiwara, K. Suenaga, T. Gregorkiewicz, Hybridization of single nanocrystals of Cs_4PbBr_6 and CsPbBr_3 . *J. Phys. Chem. C* **121**, 19490–19496 (2017). <https://doi.org/10.1021/acs.jpcc.7b05752>
 32. L. Yang, D.M. Li, C. Wang, W. Yao, H. Wang, K.X. Huang, Room-temperature synthesis of pure perovskite-related Cs_4PbBr_6 nanocrystals and their ligand-mediated evolution into highly luminescent CsPbBr_3 nanosheets. *J. Nanopart. Res.* **19**, 258 (2017). <https://doi.org/10.1007/s11051-017-3959-7>
 33. F. Iyikanat, E. Sari, H. Sahin, Thinning CsPb_2Br_5 perovskite down to monolayers: Cs-dependent stability. *Phys. Rev. B* **96**, 155442 (2017). <https://doi.org/10.1103/PhysRevB.96.155442>
 34. J.W. Xu, W.X. Huang, P.Y. Li, D.R. Onken, C.C. Dun et al., Imbedded nanocrystals of CsPbBr_3 in Cs_4PbBr_6 : kinetics, enhanced oscillator strength, and application in light-emitting. *Adv. Mater.* **29**, 1703703 (2017). <https://doi.org/10.1002/adma.1703703>
 35. Y. Bekenstein, B.A. Koscher, S.W. Eaton, P.D. Yang, A.P. Alivisatos, Highly luminescent colloidal nanoplates of perovskite cesium lead halide and their oriented assemblies. *J. Am. Chem. Soc.* **137**, 16008–16011 (2015). <https://doi.org/10.1021/jacs.5b11199>
 36. D.D. Zhang, S.W. Eaton, Y. Yu, L.T. Dou, P.D. Yang, Solution-phase synthesis of cesium lead halide perovskite nanowires. *J. Am. Chem. Soc.* **137**, 9230–9233 (2015). <https://doi.org/10.1021/jacs.5b05404>
 37. C.K. Zhou, Y. Tian, M.C. Wang, A. Rose, T. Besara et al., Low-dimensional organic tin bromide perovskites and their photoinduced structural transformation. *Angew. Chem. Int. Ed.* **56**, 9018–9022 (2017). <https://doi.org/10.1002/anie.201702825>
 38. H.L.C. Zhou, Q. He, L. Xu, M. Worku, M. Chaaban et al., Low dimensional metal halide perovskites and hybrids. *Mater. Sci. Eng.* **R137**, 38–65 (2019). <https://doi.org/10.1016/j.mser.2018.12.001>
 39. P. Zhang, G.D. Zhang, L. Liu, D.X. Ju, L.Z. Zhang, K. Cheng, X.T. Tao, Anisotropic optoelectronic properties of melt-grown bulk CsPbBr_3 single crystal. *J. Phys. Chem. Lett.* **9**, 5040–5046 (2018). <https://doi.org/10.1021/acs.jpcclett.8b01945>
 40. M.Z. Zhang, Z.P. Zheng, Q.Y. Fu, P.J. Guo, S. Zhang et al., Determination of defect levels in melt-grown all-inorganic perovskite CsPbBr_3 crystals by thermally stimulated current spectra. *J. Phys. Chem. C* **122**, 10309–10315 (2018). <https://doi.org/10.1021/acs.jpcc.8b01532>
 41. M. Rodova, J. Brozek, K. Knizek, K. Nitsch, Phase transitions in ternary caesium lead bromide. *J. Therm. Anal. Calorim.* **71**, 667–673 (2003). <https://doi.org/10.1023/a:1022836800820>
 42. F.J. Ye, W.Q. Yang, D.Y. Luo, R. Zhu, Q.H. Gong, Applications of cesium in the perovskite solar cells. *J. Semicond.* **38**, 011003 (2017). <https://doi.org/10.1088/1674-4926/38/1/011003>
 43. Q.S. Sun, C.L. Ni, Y.C. Yu, S. Attique, S.Y. Wei et al., Design principle of all-inorganic halide perovskite-related nanocrystals. *J. Mater. Chem. C* **6**, 12484–12492 (2018). <https://doi.org/10.1039/c8tc04254c>
 44. Z.J. Zhang, Y.M. Zhu, W.L. Wang, W. Zheng, R.C. Lin et al., Aqueous solution growth of millimeter-sized nongreen-luminescent wide bandgap Cs_4PbBr_6 bulk crystal. *Cryst. Growth Des.* **18**, 6393–6398 (2018). <https://doi.org/10.1021/acs.cgd.8b00817>
 45. W. Shen, L.F. Ruan, Z.T. Shen, Z.T. Deng, Reversible light-mediated compositional and structural transitions between CsPbBr_3 and CsPb_2Br_5 nanosheets. *Chem. Commun.* **54**, 2804–2807 (2018). <https://doi.org/10.1039/c8cc00139a>
 46. M. Cola, V. Massarot, R. Riccardi, C. Sinistri, Binary systems formed by lead bromide with (Li, Na, K, Rb, Cs and Tl)Br: a DTA and diffractometric study. *Zeitschrift für Naturforschung A* **26**(8), 1328–1332 (1971). <https://doi.org/10.1515/zna-1971-0812>
 47. X.S. Tang, Z.P. Hu, W. Yuan, W. Hu, H.B. Shao et al., Perovskite CsPb_2Br_5 microplate laser with enhanced stability and tunable properties. *Adv. Opt. Mater.* **5**, 1600788 (2017). <https://doi.org/10.1002/adom.201600788>
 48. L. Ruan, W. Shen, A. Wang, A. Xiang, Z. Deng, Alkylthiol ligands induced shape and crystalline phase controlled synthesis of stable perovskite-related CsPb_2Br_5 nanocrystals at room temperature. *J. Phys. Chem. Lett.* **8**, 3853–3860 (2017). <https://doi.org/10.1021/acs.jpcclett.7b01657>
 49. P.Z. Li, C.B. Hu, L. Zhou, J.T. Jiang, Y.Z. Cheng, M.L. He, X.J. Liang, W.D. Xiang, Novel synthesis and optical characterization of CsPb_2Br_5 quantum dots in borosilicate glasses. *Mater. Lett.* **209**, 483–485 (2017). <https://doi.org/10.1016/j.matlet.2017.08.079>
 50. C.J. Qin, T. Matsushima, A.S.D. Sandanayaka, Y. Tsuchiya, C. Adachi, Centrifugal-coated quasi-two-dimensional perovskite CsPb_2Br_5 films for efficient and stable light-emitting diodes. *J. Phys. Chem. Lett.* **8**, 5415–5421 (2017). <https://doi.org/10.1021/acs.jpcclett.7b02371>
 51. J.F. Lv, L.L. Fang, J.Q. Shen, Synthesis of highly luminescent CsPb_2Br_5 nanoplatelets and their application for

- light-emitting diodes. *Mater. Lett.* **211**, 199–202 (2018). <https://doi.org/10.1016/j.matlet.2017.09.106>
52. C. Han, C.L. Li, Z.G. Zang, M. Wang, K. Sun, X.S. Tang, J.H. Du, Tunable luminescent CsPb₂Br₅ nanoplatelets: applications in light-emitting diodes and photodetectors. *Photonics Res.* **5**, 473–480 (2017). <https://doi.org/10.1364/prj.5.000473>
53. P.Z. Li, Y.Z. Cheng, L. Zhou, X.Q. Yu, J.T. Jiang, M.L. He, X.J. Liang, W.D. Xiang, Photoluminescence properties and device application dots in glasses of CsPb₂Br₅ quantum dots in glasses. *Mater. Res. Bull.* **105**, 63–67 (2018). <https://doi.org/10.1016/j.materresbull.2018.04.028>
54. K.W. Wu, A. Bera, C. Ma, Y.M. Du, Y. Yang, L. Li, T. Wu, Temperature-dependent excitonic photoluminescence of hybrid organometal halide perovskite films. *Phys. Chem. Chem. Phys.* **16**, 22476–22481 (2014). <https://doi.org/10.1039/c4cp03573a>
55. L.F. Ruan, J. Lin, W. Shen, Z.T. Deng, Ligand-mediated synthesis of compositionally related cesium lead halide CsPb₂X₅ nanowires with improved stability. *Nanoscale* **10**, 7658–7665 (2018). <https://doi.org/10.1039/c8nr00883c>
56. F. Palazon, S. Dogan, S. Marras, F. Locardi, I. Nelli et al., From CsPbBr₃ nano-inks to sintered CsPbBr₃–CsPb₂Br₅ films via thermal annealing: implications on optoelectronic properties. *J. Phys. Chem. C* **121**, 11956–11961 (2017). <https://doi.org/10.1021/acs.jpcc.7b03389>
57. B. Qiao, P.J. Song, J.Y. Cao, S.L. Zhao, Z.H. Shen et al., Water-resistant, monodispersed and stably luminescent CsPbBr₃/CsPb₂Br₅ core-shell-like structure lead halide perovskite nanocrystals. *Nanotechnology* **28**, 445602 (2017). <https://doi.org/10.1088/1361-6528/aa892e>
58. S.K. Balakrishnan, P.V. Kamat, Ligand assisted transformation of cubic CsPbBr₃ nanocrystals into two-dimensional CsPb₂Br₅ nanosheets. *Chem. Mater.* **30**, 74–78 (2017). <https://doi.org/10.1021/acs.chemmater.7b04142>
59. C.K. Zhou, Y. Tian, Z. Yuan, H.R. Lin, B.H. Chen et al., Highly efficient broadband yellow phosphor based on zero-dimensional tin mixed-halide perovskite. *ACS Appl. Mater. Interfaces* **9**, 44579–44583 (2017). <https://doi.org/10.1021/acsami.7b12862>
60. C.K. Zhou, H.R. Lin, Y. Tian, Z. Yuan, R. Clark et al., Luminescent zero-dimensional organic metal halide hybrids with near-unity quantum efficiency. *Chem. Sci.* **9**, 586–593 (2018). <https://doi.org/10.1039/c7sc04539e>
61. J. Yin, P. Maity, M. De Bastiani, I. Dursun, O.M. Bakr, J.L. Bredas, O.F. Mohammed, Molecular behavior of zero-dimensional perovskites. *Sci. Adv.* **3**, e1701793 (2017). <https://doi.org/10.1126/sciadv.1701793>
62. J. Yin, Y.H. Zhang, A. Bruno, C. Soci, O.M. Bakr, J.L. Bredas, O.F. Mohammed, Intrinsic lead ion emissions in zero-dimensional Cs₄PbBr₆ nanocrystals. *ACS Energy Lett.* **2**, 2805–2811 (2017). <https://doi.org/10.1021/acsenergylett.7b01026>
63. M. De Bastiani, I. Dursun, Y.H. Zhang, B.A. Alshankiti, X.H. Miao et al., Inside perovskites: quantum luminescence from bulk Cs₄PbBr₆ single crystals. *Chem. Mater.* **29**, 7108–7113 (2017). <https://doi.org/10.1021/acs.chemmater.7b02415>
64. J. Almutlaq, J. Yin, O.F. Mohammed, O.M. Bakr, The benefit and challenges of zero-dimensional perovskites. *J. Phys. Chem. Lett.* **9**, 4131–4138 (2018). <https://doi.org/10.1021/acs.jpcclett.8b00532>
65. Y. Zhang, L. Sinatra, E. Alarousu, J. Yin, A.M. El-Zohry, O.M. Bakr, O.F. Mohammed, Ligand-free nanocrystals of highly emissive Cs₄PbBr₆ perovskite. *J. Phys. Chem. C* **122**, 6493–6498 (2018). <https://doi.org/10.1021/acs.jpcc.8b01735>
66. J.H. Cha, J.H. Han, W. Yin, C. Park, Y. Park et al., Photore-sponse of CsPbBr₃ and Cs₄PbBr₆ perovskite single crystals. *J. Phys. Chem. Lett.* **8**, 565–570 (2017). <https://doi.org/10.1021/acs.jpcclett.6b02763>
67. D.Q. Chen, Z.Y. Wan, X. Chen, Y.J. Yuan, J.S. Zhong, Large-scale room-temperature synthesis and optical properties of perovskite-related Cs₄PbBr₆ fluorophores. *J. Mater. Chem. C* **4**, 10646–10653 (2016). <https://doi.org/10.1039/c6tc04036e>
68. S. Seth, A. Samanta, Fluorescent phase-pure zero-dimensional perovskite-related Cs₄PbBr₆ microdisks: synthesis and single-particle imaging study. *J. Phys. Chem. Lett.* **8**, 4461–4467 (2017). <https://doi.org/10.1021/acs.jpcclett.7b02100>
69. Z.J. Zhang, W. Zheng, R.C. Lin, F. Huang, One-step on-chip synthesis of highly-luminescent Cs₄PbBr₆ microcrystal. *Mater. Lett.* **232**, 118–121 (2018). <https://doi.org/10.1016/j.matlet.2018.08.083>
70. W.K. Wang, D.F. Wang, F. Fang, S. Wang, G.H. Xu, T.J. Zhang, CsPbBr₃/Cs₄PbBr₆ nanocomposites: formation mechanism, large-scale and green synthesis, and application in white light-emitting diodes. *Cryst. Growth Des.* **18**, 6133–6141 (2018). <https://doi.org/10.1021/acs.cgd.8b01013>
71. Q.A. Akkerman, S. Park, E. Radicchi, F. Nunzi, E. Mosconi et al., Nearly monodisperse insulator Cs₄PbX₆ (X = Cl, Br, I) nanocrystals, their mixed halide compositions, and their transformation into CsPbX₃ nanocrystals. *Nano Lett.* **17**, 1924–1930 (2017). <https://doi.org/10.1021/acs.nanolett.6b05262>
72. X.M. Chen, F. Zhang, Y. Ge, L.F. Shi, S. Huang et al., Centimeter-sized Cs₄PbBr₆ crystals with embedded CsPbBr₃ nanocrystals showing superior photoluminescence: nonstoichiometry induced transformation and light-emitting applications. *Adv. Funct. Mater.* **28**, 1706567 (2018). <https://doi.org/10.1002/adfm.201706567>
73. M. Kepenekian, B. Traore, J.C. Blancon, L. Pedesseau, H. Tsai et al., Concept of lattice mismatch and emergence of surface states in two-dimensional hybrid perovskite quantum wells. *Nano Lett.* **18**, 5603–5609 (2018). <https://doi.org/10.1021/acs.nanolett.8b02078>
74. K. Leng, I. Abdelwahab, I. Verzhbitskiy, M. Telychko, L.Q. Chu et al., Molecularly thin two-dimensional hybrid perovskites with tunable optoelectronic properties due to reversible surface relaxation. *Nat. Mater.* **17**, 908 (2018). <https://doi.org/10.1038/s41563-018-0164-8>
75. E. Shi, S. Deng, B. Yuan, Y. Gao, Akriti et al., Extrinsic and dynamic edge states of two-dimensional lead halide perovskites. *ACS Nano* (2019). <https://doi.org/10.1021/acsnano.8b07631>
76. M.H. Du, Density functional calculations of native defects in CH₃NH₃PbI₃: effects of spin-orbit coupling and



- self-interaction error. *J. Phys. Chem. Lett.* **6**, 1461–1466 (2015). <https://doi.org/10.1021/acs.jpcllett.5b00199>
77. E. Mosconi, A. Amat, M.K. Nazeeruddin, M. Gratzel, F. De Angelis, First-principles modeling of mixed halide organometal perovskites for photovoltaic applications. *J. Phys. Chem. C* **117**, 13902–13913 (2013). <https://doi.org/10.1021/jp4048659>
78. S.B. Zhang, S.H. Wei, Nitrogen solubility and induced defect complexes in epitaxial GaAs. *N. Phys. Rev. Lett.* **86**, 1789–1792 (2001). <https://doi.org/10.1103/PhysRevLett.86.1789>
79. S.H. Wei, S.B. Zhang, Chemical trends of defect formation and doping limit in II–VI semiconductors: the case of CdTe. *Phys. Rev. B* **66**, 155211 (2002). <https://doi.org/10.1103/PhysRevB.66.155211>
80. J. Heyd, G.E. Scuseria, M. Ernzerhof, Hybrid functionals based on a screened Coulomb potential. *J. Chem. Phys.* **118**, 8207–8215 (2003). <https://doi.org/10.1063/1.1564060>
81. J. Heyd, J.E. Peralta, G.E. Scuseria, R.L. Martin, Energy band gaps and lattice parameters evaluated with the Heyd–Scuseria–Ernzerhof screened hybrid functional. *J. Chem. Phys.* **123**, 174101 (2005). <https://doi.org/10.1063/1.2085170>
82. C.W.M. Castleton, A. Hoglund, S. Mirbt, Density functional theory calculations of defect energies using supercells. *Model. Simul. Mater. Sci. Eng.* **17**, 084003 (2009). <https://doi.org/10.1088/0965-0393/17/8/084003>
83. C. Freysoldt, B. Grabowski, T. Hickel, J. Neugebauer, G. Kresse, A. Janotti, C.G. Van de Walle, First-principles calculations for point defects in solids. *Rev. Mod. Phys.* **86**, 253 (2014). <https://doi.org/10.1103/RevModPhys.86.253>
84. M.C. Brennan, J.E. Herr, T.S. Nguyen-Beck, J. Zinna, S. Draguta, S. Rouvimov, J. Parkhill, M. Kuno, Origin of the size-dependent Stokes shift in CsPbBr₃ perovskite nanocrystals. *J. Am. Chem. Soc.* **139**, 12201–12208 (2017). <https://doi.org/10.1021/jacs.7b05683>
85. V.G. Hadjiev, C. Wang, Y. Wang, X. Su, H.A. Calderon et al., Phonon fingerprints of CsPb₂Br₅. *J. Phys.: Condes. Matter* **30**, 405703 (2018). <https://doi.org/10.1088/1361-648X/aadeb4>
86. J.M. Bao, D.C. Bell, F. Capasso, J.B. Wagner, T. Martensson, J. Tragardh, L. Samuelson, Optical properties of rotationally twinned InP nanowire heterostructures. *Nano Lett.* **8**, 836–841 (2008). <https://doi.org/10.1021/nl072921e>
87. Z. Zhu, V.G. Hadjiev, Y.G. Rong, R. Guo, B. Cao et al., Interaction of organic cation with water molecule in perovskite MAPbI₃: from dynamic orientational disorder to hydrogen bonding. *Chem. Mater.* **28**, 7385–7393 (2016). <https://doi.org/10.1021/acs.chemmater.6b02883>
88. A. Dazzi, C.B. Prater, AFM-IR: Technology and applications in nanoscale infrared spectroscopy and chemical imaging. *Chem. Rev.* **117**, 5146–5173 (2017). <https://doi.org/10.1021/acs.chemrev.6b00448>
89. G. Kolhatkar, J. Plathier, A. Ruediger, Nanoscale investigation of materials, chemical reactions, and biological systems by tip enhanced Raman spectroscopy—a review. *J. Mater. Chem. C* **6**, 1307–1319 (2018). <https://doi.org/10.1039/c7tc05688e>